Research Article

Received: 27 February 2019 Revised: 14 May 2019 Accepted article published: 23 May 2019 Published online in Wiley Online Library: 17 June 2019

(wileyonlinelibrary.com) DOI 10.1002/jctb.6091

The granular capacitive moving bed reactor for the scale up of bioanodes

Casper Borsje,[a,b] Tom Sleutels,[a] Michel Saakes,[a] Cees JN Buisman[a,b] and Annemiek ter Heijne[b*]

Abstract

BACKGROUND: Scaling up bioelectrochemical systems for the treatment of wastewater faces challenges. Material costs, low conductivity of wastewater and clogging are issues that need a novel approach. The granular capacitive moving bed reactor can potentially solve these challenges. In this reactor, capacitive activated carbon granules are used as bioanode material. The charge storage capabilities of these capacitive granules allow for the physical separation of the charging and the discharging process and therefore a separation of the wastewater treatment and energy recovery process.

RESULTS: This study investigates the performance of the granular capacitive moving bed reactor. In this reactor, activated granules were transported from the bottom to the top of the reactor using a gas lift and settled on top of the granular bed, which moved downwards through the internal discharge cell. This moving granular bed was applied to increase the contact time with the discharge anode to increase the current density. The capacitive moving bed reactor (total volume 7.7 L) produced a maximum current of 23 A m^{-2} normalized to membrane area (257 A $m^{-3}_{granules}$). Without granules, the current was only 1.4 A $m^{-2}_{membrane}$. The activity of the biofilm on the granules increased over time, from 436 up to 1259 A $m^{-3}_{granules}$. A second experiment produced similar areal current density and increase in activity over time.

CONCLUSION: Whereas the produced current density is promising for further scaling up of bioanodes, the main challenges are to improve the discharge of the charged granules and growth of biofilm on the granules under shear stress.

Supporting information may be found in the online version of this article.

Keywords: capacitive bioanode; microbial electrochemical technology; bioelectrochemical system; gas lift reactor; granular bed; activated carbon

INTRODUCTION

Scaling up microbial electrochemical technologies

The focus of wastewater treatment is shifting from removal of organic material and pollutants towards the recovery of energy and nutrients. Microbial electrochemical technologies (METs) offer opportunities to recover the chemical energy from the dissolved organic material during removal. Electroactive bacteria oxidize these dissolved organics into electrons, protons and CO_2. When electroactive bacteria grow on an anode, called a bioanode, the electrons from the oxidation can be used to recover electrical energy in microbial fuel cells (MFCs), to produce products such as H_2,[1] H_2O_2,[2] and hydroxide[3,4] or to recover nutrients such as ammonia[5] and phosphate[6,7] in microbial electrolysis cells (MECs).

Although METs have been successfully operated on laboratory scale for the past decades, scaling up is still a major challenge.[8] Common strategies for scaling up are to enlarge the cell or to use multiple stacks of smaller cells.[8–13] When enlarging and stacking, the material costs increase with the reactor size, as a large part of the material costs can be allocated to the expensive electrodes[14] and ion exchange membranes, which are necessary for high performance and efficiency.[15] In general, the performance of scaled-up reactors decreases compared with lab scale.[16] One of the reasons is that conductivities of wastewaters are typically low, around 1 mS cm^{-1}.[17] The low conductivity results in lower cell voltage, due to the increased resistance of the electrolyte for ion transport.[17,18] Maintaining low distance between anode and cathode in larger reactors is challenging, especially as there is a risk of clogging.[19] Granular capacitive bioanodes have been identified as a possible solution for these challenges.[20]

Granular capacitive bioanodes

Granular capacitive bioanodes are granular activated carbon particles with an electroactive biofilm. The use of granular material

* *Correspondence to: A ter Heijne, Wageningen University, Environmental Technology, Wageningen, The Netherlands. E-mail: annemiek.terheijne@wur.nl*

This work was partially presented at the EU-ISMET 4 Conference (14 September 2018, Newcastle upon Tyne, UK)

a *Wetsus, European Centre of Excellence for Sustainable Water Technology, Leeuwarden, The Netherlands*

b *Wageningen University, Environmental Technology, Wageningen, The Netherlands*

results in a large available surface area for growth of electroactive bacteria per volume of reactor.[21,22] Activated carbon granules, in addition, contain pores, which results in a large internal surface area, allowing for formation of electrical double layers (EDLs).[23] Using the EDLs, the granules can be used to store electrons resulting from the oxidation of substrate by electroactive bacteria.[24–29] During charging, the potential decreases towards the equilibrium potential of the biocatalyzed oxidation reaction. The charged state of the granules can thus be measured via the potential of the granules. When the equilibrium potential is reached, acetate oxidation and consequent charging of the granule stops.[29] After charging, the capacitive granules can be discharged at a current collector, which is poised at a higher potential than the granules, and power is produced.[20,29] During discharge, as electrons are transferred to the current collector, cations are released to the electrolyte[20] and the potential of the granules increases.[24,29] The produced current is a combination of capacitive and faradaic current.[24,30] The release of ions is expected to increase the conductivity of the solution in the discharge cell, thereby reducing the ohmic losses and allowing for improved performance during treatment of low-conductivity wastewaters. At the same time, discharge of the granules is a requirement for growth of electroactive bacteria, as they only grow when producing current. During charging, this is directly linked to the amount of charge that can be stored in the granules, thus directly linked to the amount of charge discharged.

Fluidized granular bed systems improve mass transport of both solids and ions and are thus attractive for MET applications.[20,31] The fluidized capacitive bioanode reactor of Deeke *et al.*[20] showed that charging and discharging could be separated by transporting the charged granules from a charging reactor to an external discharge cell. Other studies used fluidization of a granular bed to make contact between capacitive granules and an anode.[32–37] Both approaches resulted in limited current density, likely due to short contact time of the granules with the current collector. Therefore this study aims to investigate the effect of prolonged contact times on current production. Longer contact times of the capacitive granules with a current collector require a different reactor type and design. Instead of a fluidized reactor, we therefore designed and operated a moving bed reactor. This reactor type allows for granules to move through a discharge cell in a semi-packed bed, where the granules have longer contact with the current collector compared with a fluidized system.[38]

In the moving bed reactor, with a total volume of 7.7 L, capacitive bioanode granules were circulated using a gas lift and settled down on a moving granular bed. The performance of the moving bed reactor was studied under ideal conditions: non-limiting acetate concentrations, constant pH and with inhibition of methanogenic activity. Two independent experiments were performed. Granules were harvested regularly to monitor activity of the electroactive biofilm in a separate test cell, as well as to study the presence of biofilm on the electrode with scanning electron microscopy.

MATERIALS AND METHODS

Reactor

A novel design for a granular capacitive moving bed bioanode was developed where activated carbon granules circulated using a gas lift and settled through an internal discharge cell. This new reactor design was based on the continuous sand filter reactors,[39] which circulate sand particles, commercially known as Dynasand by Nordic Water (https://www.nordicwater.com/product/dynasand/), in order to create a moving granular bed.

Reactor design

The reactor consisted of a poly(vinyl chloride) (PVC) tube of 138 cm length with a diameter of 95.4 mm. This tube was divided in five sections (Fig. 1A): the top section, the main column, the funnel section with the discharge cell, the conical bottom and the gas lift tube. The total reactor had an anode volume of 7.7 L (both liquid and granules) and a cathode volume of 300 mL, both excluding the recirculation volumes (470 and 250 mL respectively). A scaled drawing of the design with associated recirculation volumes and flows can be found in Fig. A1 of 'Supporting information' (SI).

The main column held the bulk of the liquid and allowed the granules to settle down towards the funneled section, which narrowed the flow path, in radius, from 39.7 mm (between outer tube and gas lift of 16 mm) to 8 mm in the discharge cell. The discharge cell consisted of five concentric parts, which are from inside to outside: the flow channel, the discharge anode, the membrane on its support structure, the cathode and the cathode compartment. Figure 1B shows a zoom to the discharge cell construction and Fig. 1C shows a cross-section of the discharge cell.

The flow channel was created by an insert, made from PVC, and the discharge anode. The discharge anode (2 mm thick titanium mesh 1.4 coated with Pt/Ir mixed metal oxide (MMO), Magneto Special Anodes B.V., Schiedam, Netherlands) had a mesh structure 10 cm long (1/14th of the total reactor length), which allowed anolyte access to the membrane for ionic contact. The volume in the flow channel, for the moving granule bed, next to the mesh part of the discharge anode was 163 cm^3. The cation exchange membrane (Ralex CM-PP, MEGA a.s., Stráž pod Ralskem, Czech Republic) was fixed on an open-structured PVC support (121 holes), which resulted in 137 cm^2 effective membrane area. The cathode (same make as discharge anode) was on the outside of the membrane. An injectable gasket (Repliset F5, Streurer GmbH Nederland, Maassluis, Netherlands) was used to seal the membrane and electrodes.

Below the discharge cell, the reactor was shaped as a funnel (from 95.4 to 20 mm diameter). A Luggin-Haber capillary was inserted into the reactor here to connect a reference electrode. The bottom of the funnel led to the opening of the gas lift, which has an inner diameter of 9 mm. The gas lift ended just below the water level at the top of the reactor. The top section facilitated separation of solids, gas and liquid. The anolyte overflowed into the recirculation volume, where the gas and liquid effluent were separated.

The reactor contained 1200 mL (584 g dry weight, in the first experiment) and 2415 mL (1174 g dry weight, in the second experiment) of activated carbon granules (density 0.486 g cm^{-3}, coconut shell-based HR5, Eurocarb, Bristol, UK), sieved to size between 0.5 and 0.8 mm (stainless steel sieves, VWR, Amsterdam, Netherlands). The porosity was measured at 1100 $m^2\ g^{-1}$ specific surface area for pore width range 0.3–50 nm (two-dimensional non-local density functional theory (2D-NLDFT) model applied to N_2 adsorption measurements at 77 K using TriStar 3000, Micromeritics B.V., Veldhoven, Netherlands). At the bottom of the reactor, anolyte and granules were transported up by the gas lift. After exiting the gas lift tube, the granules settled down in the main volume, on top of the granule bed. In this way, a moving bed of capacitive granules was created that moved downwards through the discharge cell. This continuously settling bed of granules moved through the 8 mm wide channel, resulting in a particle bed in contact with the discharge anode. The circulation cycle is completed as

Journal of Chemical Technology & Biotechnology published by John Wiley & Sons Ltd on behalf of Society of Chemical Industry.

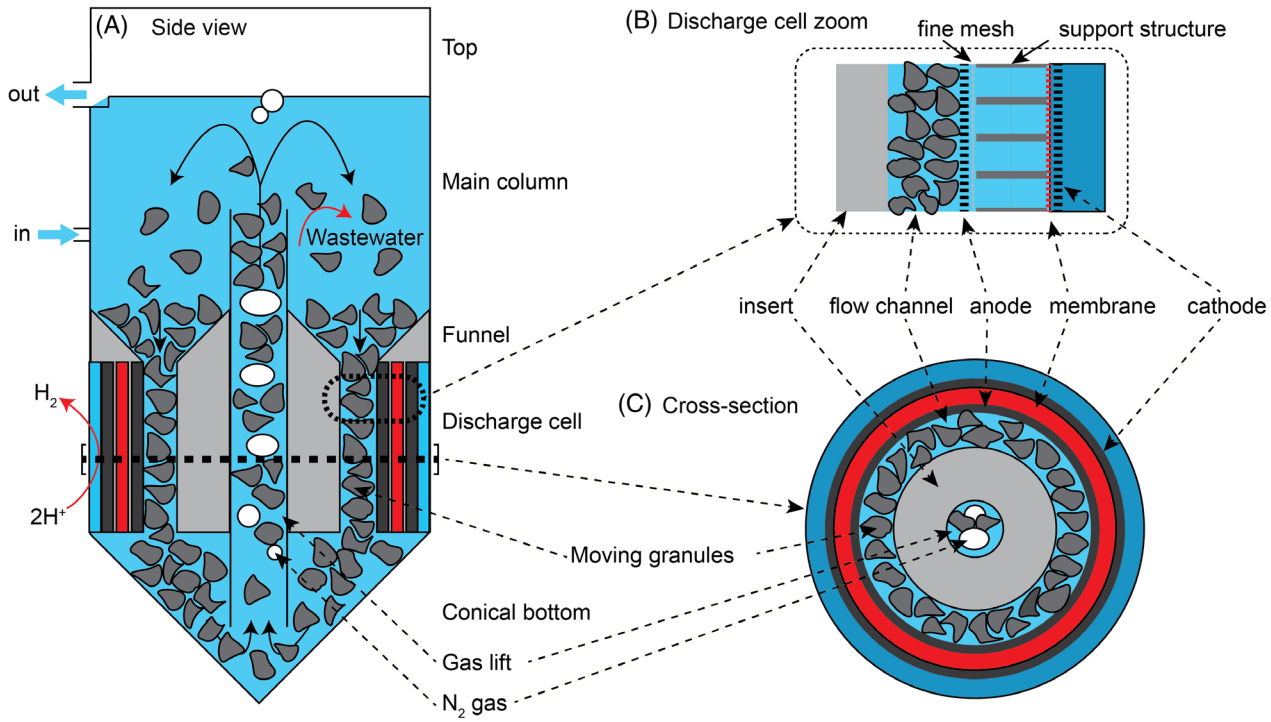

Figure 1. (A) Schematic overview of the reactor with its five sections. The red arrows indicate the oxidation and reduction reactions, while the solid black arrows indicate the flow of the granules. (B) Detail of the discharge cell. (C) Cross-section of the discharge cell.

the granules settle towards the bottom of the gas lift, where the conical shape of the bottom centers the granule flow to the gas lift.

N_2 flow to the gas lift was supplied via a mass flow controller (Mass-Stream, Bronkhorst Nederland B.V., Veenendaal, Netherlands) to provide a steady flow of granules. The use of N_2 also ensured an anoxic environment. Granule flow measurements from the top of the gas lift (see Fig. B1 of SI) showed that the residence time of the granules in the discharge cell was between 27 and 52 s for 500–300 mL min^{-1} of N_2 flow (Section B of SI). Change in flow rate was not observed to affect the current density on the long term.

Measurements in the reactor

Dissolved oxygen (DO) (SE 715, Knick, Berlin, Germany) and pH (CPS71 and CPS11D, Endress+Hauser B.V., Naarden, Netherlands) were measured online in the anolyte recirculation. The anolyte pH was controlled at 6.9 ± 0.3 (Liquiline, Endress+Hauser B.V., Naarden, Netherlands) through NaOH dosing into the circulation, which was pumped at 150 mL min^{-1} (same rate for the catholyte). A heating jacket around the main tube heated the anolyte to 28 °C using a water bath (Immersion Circulator DC10, Thermo Fisher Scientific, Breda, Netherlands).

The charged state of local granules (see introduction), before entering the discharge cell, was measured as the $E_{granules}$ potential using a Pt/Ir wire (0.25 mm diameter, 80:20 ratio Pt/Ir, Advent-RM, Oxford, UK) and a reference electrode in close proximity. The potential of the wire represented the potential of the granules, as the wire takes the same potential as granules when they collide with the wire. The wire was removed for regular cleaning from biofilm growth.

Granular activity test cell

To determine the change in activity of the electroactive bacteria growing on the granules, a small volume of granules from the reactor was taken regularly with three replicates per day. These granules were placed in a small test cell. Figure 2A shows a schematic view of the granules in the test cell and Fig. 2B a photo of the test assembly. The activity test cell consisted of a 6 mm diameter titanium electrode (contact surface coated with Pt/Ir MMO, Magneto Special Anodes B.V., Schiedam, Netherlands), which was screwed against the granules at 40 N cm (TorqueVario-S 36849, Wiha, Werkzeuge GmbH, Schonach, Germany) in a polymethyl methacrylate (PMMA) housing. The cathode was a Pt/Ir wire in the electrolyte. The electrolyte and experimental conditions were the same as in the anode side of the reactor.

Inoculum and medium

As inoculum, a mixed electroactive community was taken from an MEC in our laboratory. This cell was running on acetate, used methanogen inhibitor (sodium 2-bromoethanesulfonate (Na 2-BES)) and operated at a controlled anode potential of −0.35 V *vs* Ag/AgCl.[40] The granules were used with inoculum during the testing phase of the reactor, which will have resulted in an initial activity by biofilm on the granules.

The influent was continuously supplied in the middle of the main column to the reactor, resulting in a hydraulic retention time (HRT) of 35 ± 3 h (volume for HRT includes recirculation volume). The influent was fed through mixing (1:1) of carbon source and nutrient source from two different vessels, preventing microbial growth in the influent. The carbon source vessel contained potassium phosphate buffer (10 mmol L^{-1} K_2HPO_4 and 10 mmol L^{-1} KH_2PO_4), acetate (the first experiment had 20 mmol L^{-1} in the start-up phase and 40 mmol L^{-1} at day 14; the second experiment was started with 40 mmol L^{-1}) and 20 mmol L^{-1} Na 2-BES. Acetate was measured using ion chromatography (761 Compact IC, Metrohm, Herisau, Switzerland, with column 00G-4375-E0, Phenomenex, Utrecht, Netherlands). The nutrient source contained

Journal of Chemical Technology & Biotechnology published by John Wiley & Sons Ltd on behalf of Society of Chemical Industry.

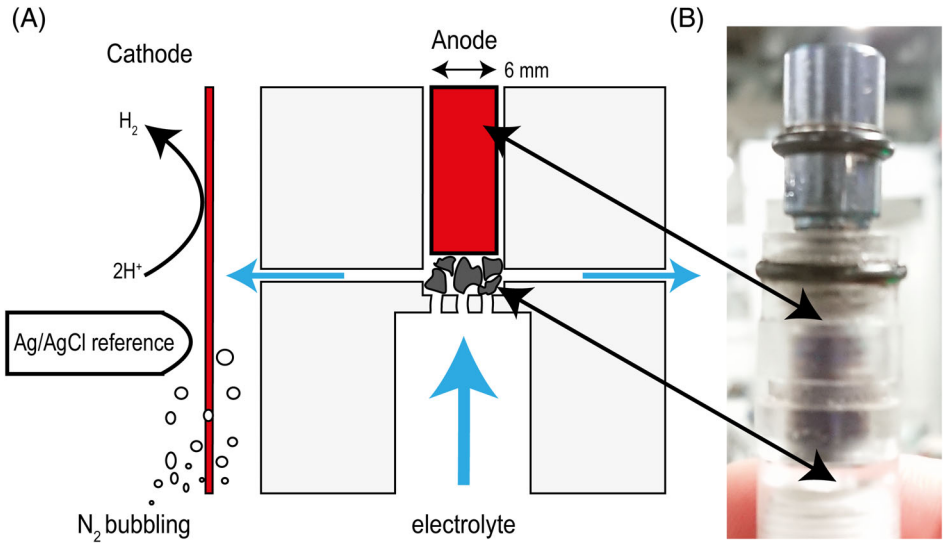

Figure 2. (A) Schematic of the granular activity test cell where a small batch of granules could be tested for bioanode activity. The granules were pressed between the cell and the anode (blue arrows indicate electrolyte flow). (B) Photo of the test assembly.

20 mmol L^{-1} KCl, 20 mmol L^{-1} NaCl, 10.4 mmol L^{-1} NH_4Cl, 1.4 m $CaCl_2$, 80 µmol L^{-1} $MgSO_4$ and 0.2 mL L^{-1} trace metal solution.[41] The chemical compounds were obtained from VWR. The influent solutions were continuously sparged with N_2. The catholyte consisted of a 40 mmol L^{-1} phosphate buffer solution (20 mmol L^{-1} K_2HPO_4 and 20 mmol L^{-1} KH_2PO_4) and was continuously supplied to keep the catholyte pH below 12. This prevented degradation of the sealing gaskets.

Electrolyte for the activity test cell was the same as the influent for the reactor and used for all measurements during 1 day.

Electrochemical methods

All electrochemical methods were performed using potentiostats in a three-electrode setup (IviumStat for the reactor and Ivium-n-Stat for the test cell, Ivium Technologies, Eindhoven, Netherlands). All potentials were controlled or measured against an Ag/AgCl/3 mol L^{-1} KCl reference electrode (+205 mV *vs* SHE, QM711X/GEL, Prosense B.V., Oosterhout, Netherlands). Reference electrodes for the reactor were connected using Luggin-Haber capillaries (QM715X/4X50/CF, Prosense, Oosterhout, Netherlands) (filled with 3 mol L^{-1} KCl), while the reference electrode for the activity test cell was placed directly in the main volume.

Currents and potentials were measured every 60 s for the reactor and every 1 s for the activity test cell. To prevent oscillation in the potentiostat control, due to the capacitive character of the reactor, a high-frequency shunt (3 × 100 µF in series, Multicomp MCCB1E107M2FCB, Farnell (Netherlands) B.V., Utrecht, Netherlands) was attached between reference and counter electrode.

Control of the discharge anode in the reactor

The discharge anode was controlled at an applied anode potential followed by a period of applied current. The anode potential control was used to harvest the electrons at constant energy level (common procedure in MFC operation), while applied (forced) current was used to force discharge of the capacitive granules, as increased discharge of the granules will increase both the capacitive current and biological activity of the reactor (see above for more details). Figure 3 shows examples of the control method for the discharge cell. The discharge anode potential was controlled at 0 V *vs* Ag/AgCl for 1 h, followed by current control for 1 h or until +0.15 V *vs* Ag/AgCl was reached. During the experimental procedure, the current was controlled at three different levels, depending on the performance of the reactor: +7.3, +10.9 and +14.6 A m^{-2} on top of the last measured current. The applied current resulted in an increase in anode potential. The current control period was aborted when the anode potential increased past +0.15 V *vs* Ag/AgCl, to prevent unwanted electrochemical reactions, or maintained for a maximum period of 1 h if the anode potential remained below +0.15 V *vs* Ag/AgCl. This sequence was performed throughout the whole experiment (unless stated otherwise).

Activity test control

The activity of the capacitive granules was measured in a polarization curve as the current produced at −0.1, −0.2 and −0.3 V *vs* Ag/AgCl. For one data point, the last 10 s of 10 min applied potential were averaged and the current was normalized to the volume of dry granules (via the bulk density and the dry weight, after washing three times with Milli-Q water and drying overnight at 105 °C). To ensure positive currents only, the granules were charged to −0.4 V *vs* Ag/AgCl or lower (except where noted differently). For activity tests, the faradaic charging current decreased the potential at open cell potential (OCP) (see above).

Scanning electron microscopy

A sample of granules was taken from the reactor at the point where they were settling in the main column. Fixation for scanning electron microscopy (SEM) analysis (JSM-6480LV, JEOL (Europe) B.V., Nieuw-Vennep, Netherlands) was performed with 24 h at 4 °C in 6.25% (v/v) glutaraldehyde in phosphate-buffered saline (PBS 1x Dulbecco's, A0965, AppliChem GmbH, Darmstadt, Germany), filtered over 0.22 µm. The granules were then washed three times for 15 min with PBS (filtered over 0.22 µm), for 20 min with 30, 50, 70 and 90% (v/v) ethanol and twice for 30 min with 96% (v/v) ethanol, dried at 40 °C for a minimum of 1 h and stored in closed bottles at room temperature.

Journal of Chemical Technology & Biotechnology published by John Wiley & Sons Ltd on behalf of Society of Chemical Industry.

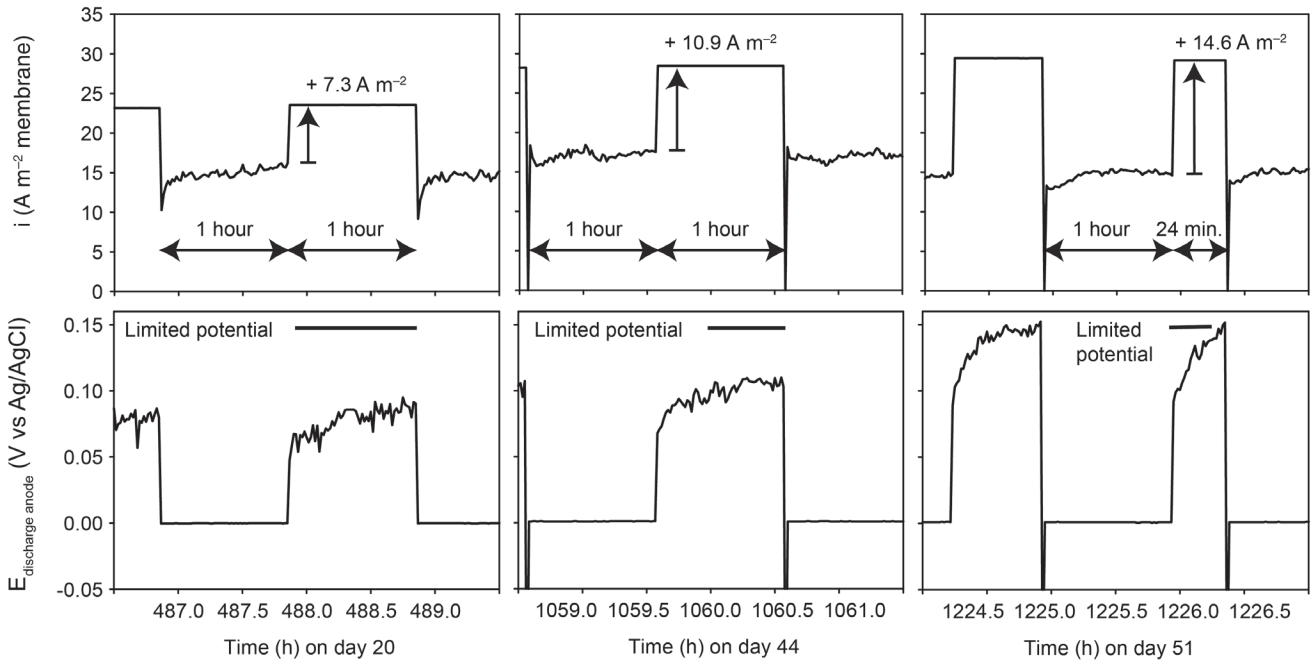

Figure 3. The discharge cell was controlled by controlling the anode potential at 0 V *vs* Ag/AgCl for 1 h and then controlling the current at an applied current, lasting either 1 h or until an anode potential of +0.15 V was reached. In this figure, examples are shown for the three applied current controls used in the first experiment.

RESULTS AND DISCUSSION

The reactor showed stable performance

Figure 4 shows the current density of the reactor per membrane area in the discharge cell of the first (Fig. 4A) and second (Fig. 4B) experiments. The behavior of the current over time will be discussed in combination with the results of the granule activity (see below). In the first experimental run, the average daily current density ranged between 10 and 23 A $m^{-2}_{membrane}$ during 66 days of reactor operation. During the first 8 days, the daily average current density increased from 10 to 19 A m^{-2}. From day 33 on, the controlled current was increased to +10.9 A m^{-2} (see methodology for more details on the potential–current control cycle). Over the course of the following 12 days, the daily average current increased to a stable maximum of 23 A m^{-2} (day 44), with a maximum of 17 A m^{-2} during potential control. Further increase of the controlled current to +14.6 A m^{-2} (day 45 to 54) resulted in the highest daily average current of 25 A m^{-2} on day 46, after which the current density decreased to 20 A m^{-2}. At an applied current of +10.9 A m^{-2} from day 54 onward, the daily average current increased again to 21 A m^{-2}. After 66 days, the acetate feed was stopped, the results of which will be shown and discussed in more detail below. The experiment was concluded by removing the granules (day 73) to investigate if the current was indeed produced from the granules. The daily average current produced by the discharge anode without granules (and 16 mmol L^{-1} acetate) was 1.4 A $m^{-2}_{membrane}$; as this current is only 9% of the current obtained with granules, at the same discharge anode potential, the granules contributed to most of the current in the moving bed reactor.

A second experiment was performed for 33 days under similar conditions, though with 2415 mL of unused granules (as compared with the pre-used granules used in the first experiment; see methodology), and resulted in comparable current densities to the first experiment, with a maximum daily average of 21 A m^{-2}, and 17 A m^{-2} under potentiostatic control. The current increased rapidly to 10 A m^{-2} in the first 5 days, as the unused granules started up as a bioanode, after which the maximum of 21 A m^{-2} was reached on day 16. Afterwards, there was trouble in controlling the system. The current density never increased to previous levels and the experiment was terminated. Owing to the troubles with the system, the applied current did not exceed +7.3 A m^{-2}.

The current data recorded per minute show a large variation. This variation is the result of the discharge method of sequential potential control and current control: the current measured during controlled potential is always lower than the applied current, which was controlled at a higher value to force higher rates (see methodology). A second reason for the variation is the intermittent contact of granules with the discharge anode, releasing a varying amount of charge per minute. Peaks such as on days 2, 20, 28, 35, 45 and 47 (first experiment) and day 13 (second experiment) are due to maintenance, where a capacitive peak occurred after a short OCP period. Other peaks after day 16 in the second experiment were due to continued trouble in the system.

Although the current density per membrane area is similar for both experiments, the second experiment was performed with double the volume of granules of the first experiment. This means that the areal current density (A m^{-2}) remained the same while the granular current density (A $m^{-3}_{granules}$) halved. This indicates there is an optimum ratio of granules to discharge anode surface area. This optimum is related to the earlier studied ratio of charging to discharging time[24,25,42,43]: the charging time is the time the granules are outside the discharge cell, which increases with more granules, and the discharging time is the time the granules are in contact with the discharge anode.

The activity of the granules increased over time

The activity of the electroactive bacteria on the granules was measured throughout the experimental periods. A small amount

Journal of Chemical Technology & Biotechnology published by John Wiley & Sons Ltd on behalf of Society of Chemical Industry.

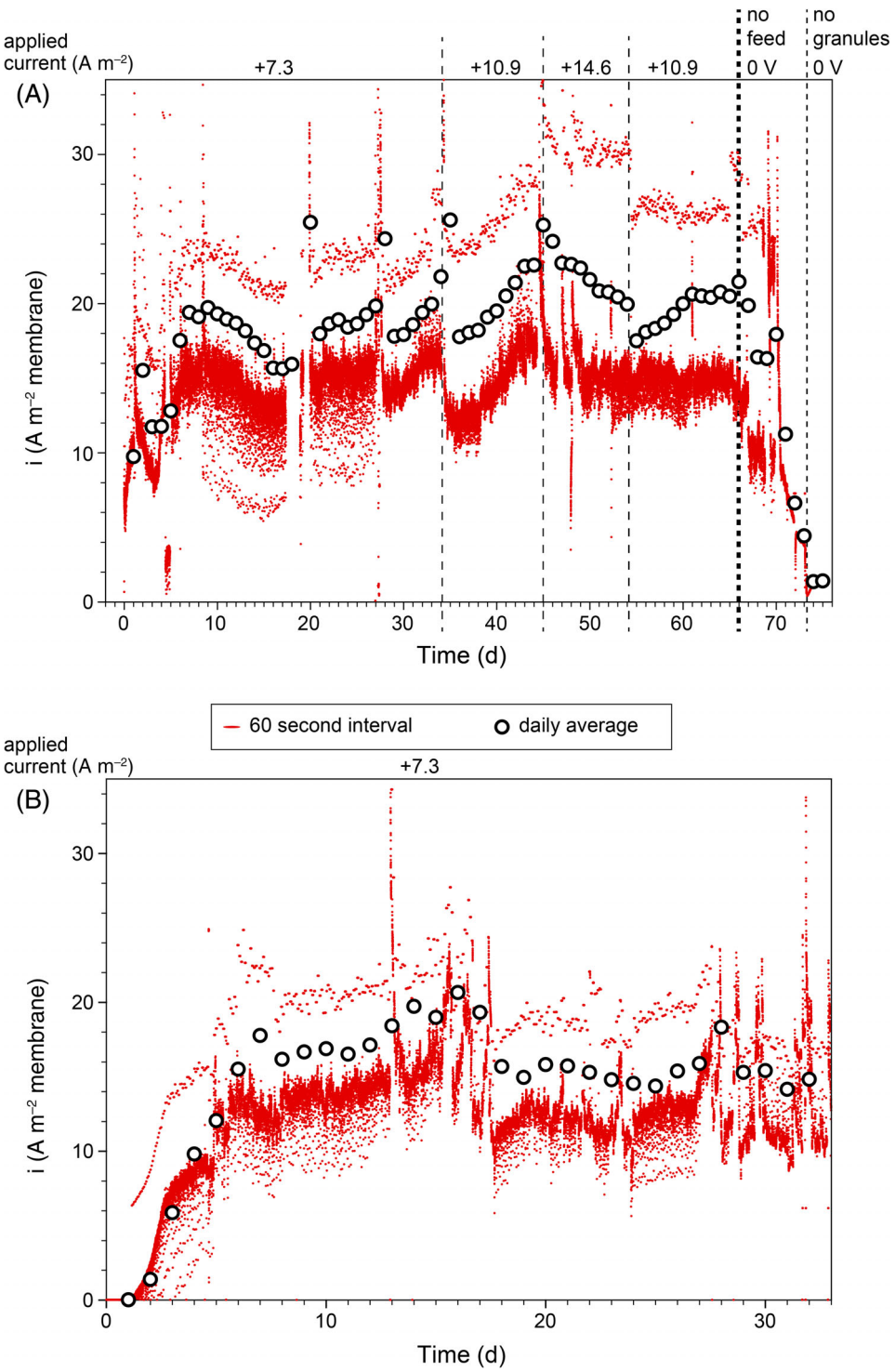

Figure 4. The current density results, normalized to the membrane area in the reactor, of (A) the first experiment and (B) the second experiment. The small red dots show the data per minute, while the open circles show the daily average. In A, the different periods of control are indicated with the dashed lines. On top of the figure are the different applied currents in the potential–current control cycles, where e.g. +10.9 A m^{-2} was applied on top of the last measured current at controlled potential. The thin dashed lines indicate the changes in applied current. In the second experiment, only + 7.3 A m^{-2} was used. The thick dashed line indicates the end of the main experiment. Open circuit data are not displayed for clarity of the figure.

of granules (16 ± 5 mg) was taken from the reactor regularly. Figure 5 shows the current density of the granules over time, normalized to granule volume, at three controlled potentials used in the polarization curve for the first (Fig. 5A) and second (Fig. 5B) experiments.

For both experiments, there is a clear increase in the activity. For the first experiment, at an anode potential of −0.1 V *vs* Ag/AgCl, the current increased from 436 A $m^{-3}_{granules}$ (averaged over the first 10 days) to 1259 A $m^{-3}_{granules}$ (average of last two measurement days), showing a 2.9 times increase in current density over the

Journal of Chemical Technology & Biotechnology published by John Wiley & Sons Ltd on behalf of Society of Chemical Industry.

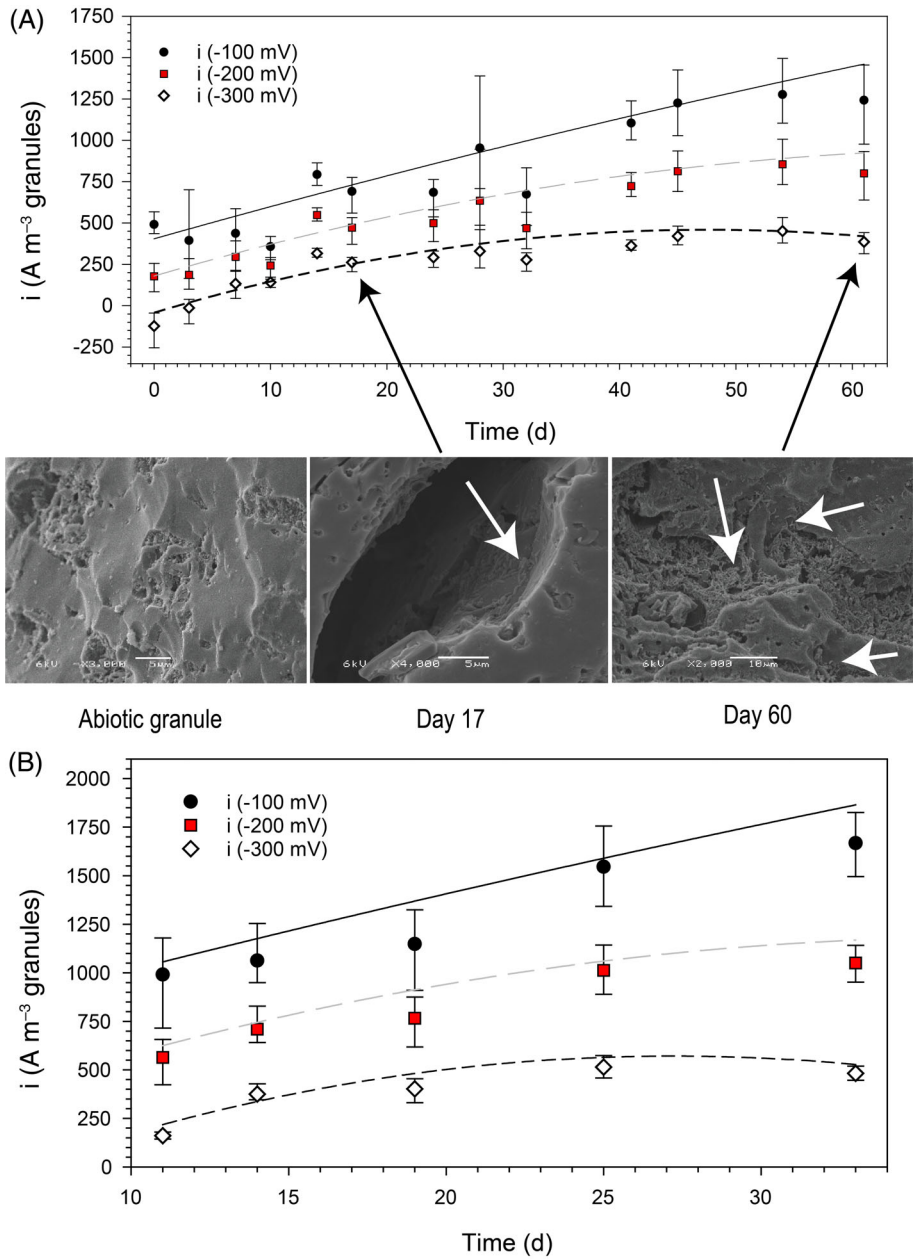

Figure 5. Activity of the granules in the test cell at three anode potentials: black circles, −100 mV *vs* Ag/AgCl; red squares, −200 mV *vs* Ag/AgCl; open diamonds, −300 mV *vs* Ag/AgCl. (A) The first experiment and (B) the second experiment. The current density is expressed as volume of granules at the discharge anode in the test cell (dry weight into volume of granules). The lines are added to guide the eye. The SEM images show the increased amount of biofilm on the granules over time, with the white arrows pointing to concentrations of microorganisms.

experimental period. During the first 3 days, the negative current at −0.3 V *vs* Ag/AgCl during this time shows that the anode potential in the test cell was lower than the granule potential of the sample: the granules in the reactor had not been fully charged yet.

The increase in activity with time is in line with the reactor performance: the current density of the granules in the test cell and in the reactor increased until around day 45 and stagnated after that time until the end of the first experiment. In the second experiment, the activity increased by 1.6 times until day 25. After day 25, the activity stagnated, similar to the reactor performance and similar to the behavior in the first experiment.

As both reactors show stagnating activity over time simultaneous with a stagnating current density in the reactor, the stagnating current density is likely the result of limited coverage of granules by electroactive biofilm. We propose two mechanisms occurring simultaneously: (i) shear stress on the biofilm and (ii) insufficient discharging of the granules, which is directly linked to growth (see introduction).

Shear stress on the biofilm

The shear stress on the outer surface of the granules was caused by the constant movement of the granular bed. SEM images taken of granules from the reactor indeed show limited growth on the granule surface. Figure 5A shows SEM images of granules from the first experiment in three different states of growth: clean, day 17 and day 60. Three important observations can be made based

Journal of Chemical Technology & Biotechnology published by John Wiley & Sons Ltd on behalf of Society of Chemical Industry.

on these images: (1) biofilm is formed in the large pores on the granule surface; (2) biofilm development increased in the period in which activity of the biofilm on the granules increased; (3) the outer surface of the granules was devoid of microorganisms, probably because of shear stress. Thus the shear stress affected the total amount of biofilm present on the granules, which limits the faradaic contribution to the total current produced by the granules during discharging.

Insufficient discharging of the granules

Figure 6 shows the measured current, open circuit granule potential and acetate concentration after feeding of the system was stopped at the end of the first experiment. When the acetate concentration decreased below the detection limit of 0.01 mmol L^{-1}, the current decreased. At the same time, the granule potential ($E_{granules}$) measured above the discharge cell increased. Since the potential of the granules is linked to the stored charge (see introduction), the increase in granule potential shows that the granules were slowly releasing electrons to the discharge anode. The discharging period in the reactor is equal to the residence time of the granules in the discharge cell, which is between 27 and 52 s (see methodology). This is many times shorter than the multiple days that were required here to discharge without acetate feeding, and a clear indication that the discharging is limiting the current produced by the reactor.

Improving the discharging will not only improve the growth and activity of the biofilm but also increase the total current, as more charge is transferred during discharge. Thus improving the discharge of the granules is essential to exploit the reactor's maximum performance.

Perspectives for application of the granular capacitive moving bed reactor

Comparison with other granular bioanode systems

Table 1 shows the results of the current density of the moving bed reactor in comparison with other experimental studies using granular bioanode systems. Here we present the current density normalized to granule volume to compare with the other granular bioanodes. The current density per projected membrane area or projected cathode area is also shown in order to compare the current density of the discharge cell with other systems' cell designs.

The moving bed reactor produced a maximum of 257 A $m^{-3}_{granules}$ (daily average) during the first experiment. If normalized to the volume of the discharge cell, this is 1891 A $m^{-3}_{granules}$ or 7 times higher than when normalized to the total volume of granules in the reactor. The granules from the reactor produced 1667 A $m^{-3}_{granules}$ at −0.1 V *vs* Ag/AgCl as a fixed bed in the activity test cell during the second experiment. These results are comparable to the 1495 A $m^{-3}_{granules}$ produced by a non-capacitive granular packed bed at 0 V *vs* Ag/AgCl.[44] The comparison between current density per total volume of granules in the reactor and granule volume in the discharge cell shows again that there is an optimum ratio of granules to discharge anode surface (see above). Still, compared with the best performing capacitive bioanode, at −0.3 V *vs* Ag/AgCl, the performance in the test cell (482 A $m^{-3}_{granules}$ in the second experiment) was 159 times lower than measured for a single activated carbon granule fixed to a Pt wire (76 765 A $m^{-3}_{granule}$) at the same potential.[29]

Other capacitive bioanodes with intermittent contact were either fluidized for contact with the discharge anode[32–37] or fluidized before flowing through an external discharge cell.[20] The fluidization by stirring the granular activated carbon in the study by Liu *et al.*[35] produced 1603 A $m^{-3}_{granules}$, similar to the moving granules in the discharge cell of the moving bed reactor; however, this system was several times smaller. Compared with the fluidized bed reactor with an external discharge cell,[20] the moving bed through the discharge cell increased the areal current density 17 times.

The fluidized capacitive bioanode studied by Tejedor-Sanz *et al.*[37] produced the highest current density per granule volume so far: 214 A $m^{-3}_{granules}$ at +0.2 V *vs* Ag/AgCl. The moving bed reactor produced a maximum of 257 A $m^{-3}_{granules}$ (daily average over the potential–current control cycles). If only the periods of potential control are considered, the reactor produced a maximum of 215 A $m^{-3}_{granules}$ at 0 V *vs* Ag/AgCl. It is generally considered that increased scale leads to lower current density. Thus it is interesting to notice that in the moving bed reactor the result was achieved with 1200 mL of granules as compared with 80 mL of granules in the fluidized bed of Tejedor-Sanz *et al.*,[37] i.e. comparable granular current density using more granules. Normalization to the projected surface area shows that our reactor had a 10 times higher areal current density, therefore a higher current density was produced using fewer materials. These results are promising for scale up of bioanodes using moving bed capacitive bioanodes.

Conclusions and strategies for improving the reactor towards application

In this paper, we focused on improving the contact time of the granules with the discharge anode. The granular capacitive moving bed reactor has shown promising results with regards to scaling up bioanodes. The granular capacitive moving bed reactor produced 23 A $m^{-2}_{membrane}$ (257 A $m^{-3}_{granules}$), showing stable performance for 66 days and an increase in activity on the granules over time. The granular current density is similar to smaller-scale fluidized capacitive bioanodes, which is promising for scale up of bioanodes. Analysis of the results shows the limitations of the reactor: (1) the shear stress on the biofilm on the granule surface imposed limitations on the faradaic current and (2) the capacitive current is limited in the reactor, as evident from the slow discharging without recharging. Aside from this, the results show that there is an optimum ratio of granules per discharge anode surface area: the areal current density was similar between the two experiments, but normalization to the granule volume halved the current density. The same conclusion was drawn via normalization of the produced current to the discharge cell granule volume, which showed 1891 A $m^{-3}_{granules}$, i.e. 7 times higher than 257 A $m^{-3}_{granules}$ in the reactor.

Strategies to tackle the main challenges, i.e. limited capacitive current and limited biofilm coverage on the granules, are necessary to increase the current density. To increase coverage of the biofilm, granules should be chosen or engineered to provide protection from shear stress. However, some application of shear might be beneficial for removal of methanogenic bacteria which often grow on the outside of bioanode biofilms.[45] Optimizing the available surface for biofilm growth, protected from shear stress but still allowing removal, would allow for higher faradaic current to add to the capacitive current. The capacitive current depends on the material properties of the activated carbon granules, as previous experiments have shown.[29] Material properties such as porosity,[46–49] surface roughness,[50–53] surface chemistry[54,55] and material conductivity all play a role in the produced current. Material conductivity is an important factor, as decreasing the resistance of the granules will improve the charge transfer of

Journal of Chemical Technology & Biotechnology published by John Wiley & Sons Ltd on behalf of Society of Chemical Industry.

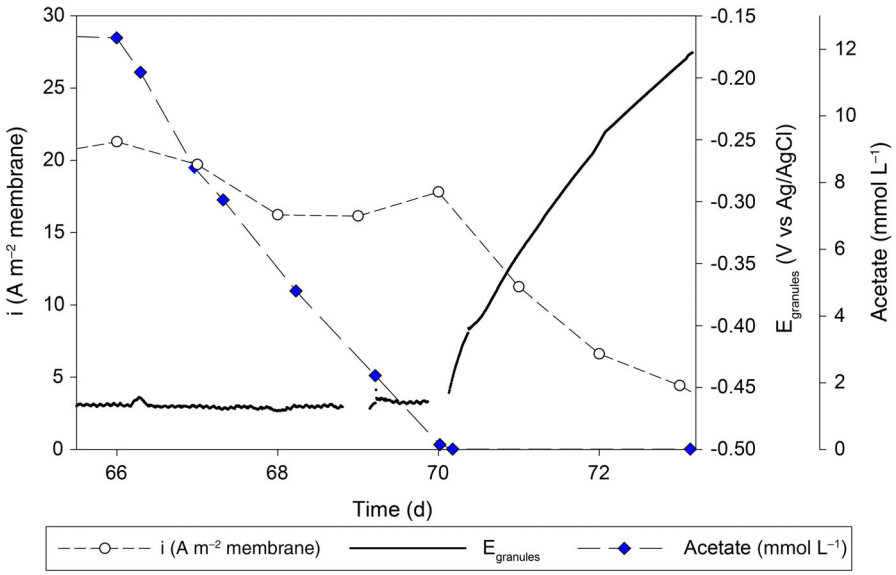

Figure 6. The current density (short dashed line with open circles) of the reactor in the period without feeding the system. The increase in the potential $E_{granules}$ (solid black line) shows the discharging process when the charging process is limited by the low acetate concentration (long dashed line with blue diamonds).

Table 1. An overview of previously studied granular bioanode systems for comparison with the granular capacitive moving bed reactor

System	A (cm^2)	V (mL)	$V_{granules}$ (mL)	i (A m^{-2})	i (A m^{-3} granules)	i (A m^{-3} reactor)	Reference
Non-capacitive bioanodes							
Packed bed cell	– [a]	156	111	– [a]	1495	1063	44
Capacitive bioanodes							
Fixed single granule	1.3[b]	1	0.01	5.7	76 765	757	29
Fluidized bed cell	0.8[c]	40	2.3	2.6	89	5	35
Fluidized bed cell[d]	7[c]	7	1.1	2.6	1603	260	32
Fluidized bed reactor[d]	719[b]	1000	300	0.2	37	11.1	36
Fluidized bed reactor[d]	3.1[c]	1000	177	1.3	2.3	0.4	34
Fluidized bed reactor	11[b]	2102	392	1.3	3.6	0.7	20
Fluidized bed reactor	70[c]	680	80	2.4	214	25.2	37
Moving bed reactor[e]	137[b]	7700	1200	22.6	257	40.1	This study
Moving bed discharge cell[e]	137[b]	163	163	22.6	1891	1891	This study
Fixed bed activity[f]	– [a]	– [a]	0.024	– [a]	1667	– [a]	This study

[a] Unknown or not determined.
[b] Projected surface area of the membrane.
[c] Projected surface area of the cathode.
[d] Current density for maximum power.
[e] First experiment.
[f] Second experiment.

highly capacitive granules. Choosing granules with the right properties or engineering granules for reduced resistance will change the optimum volume of granules in the reactor.

After engineering granules for lower resistance and improved protection against shear stress for the biofilm, a study into the optimal ratio of granules to discharge anode surface area should be performed. Finally, the results presented in this study were obtained in ideal conditions, i.e. acetate as substrate, pH control and sufficient buffer capacity. Therefore the moving bed reactor should be studied in real conditions such as real wastewater, limited buffer capacity and minimum addition of chemicals. The improvements and experience with real conditions are needed to realize the full potential of the granular capacitive moving bed reactor.

ACKNOWLEDGEMENTS

This work was performed in the cooperation framework of Wetsus, European Centre of Excellence for Sustainable Water Technology (www.wetsus.eu). Wetsus is co-funded by the Dutch Ministry of Economic Affairs and Ministry of Infrastructure and Environment, the European Union Regional Development Fund, the Province of Fryslân and the Northern Netherlands Provinces. The authors thank the participants of the research theme 'Resource Recovery' for the fruitful discussions and their financial support.

Supporting Information

Supporting information may be found in the online version of this article.

REFERENCES

1 Rozendal RA, Hamelers HVM, Euverink GJW, Metz SJ and Buisman CJN, Principle and perspectives of hydrogen production through biocatalyzed electrolysis. *Int J Hydrogen Energy* **31**:1632–1640 (2006). https://doi.org/10.1016/j.ijhydene.2005.12.006.

2 Rozendal RA, Leone E, Keller J and Rabaey K, Efficient hydrogen peroxide generation from organic matter in a bioelectrochemical system. *Electrochem Commun* **11**:1752–1755 (2009). https://doi.org/10.1016/j.elecom.2009.07.008.

3 Sleutels THJA, Hamelers HVM and Buisman CJN, Reduction of pH buffer requirement in bioelectrochemical systems. *Environ Sci Technol* **44**:8259–8263 (2010). https://doi.org/10.1021/es101858f.

4 Logan BE and Rabaey K, Conversion of wastes into bioelectricity and chemicals by using microbial electrochemical technologies. *Science* **337**:686–690 (2012). https://doi.org/10.1126/science.1217412.

5 Kuntke P, Sleutels THJA, Rodríguez Arredondo M, Georg S, Barbosa SG, ter Heijne A *et al.*, (Bio)electrochemical ammonia recovery: progress and perspectives. *Appl Microbiol Biotechnol* **102** :3865–3878 (2018). https://doi.org/10.1007/s00253-018-8888-6

6 Cusick RD and Logan BE, Phosphate recovery as struvite within a single chamber microbial electrolysis cell. *Bioresour Technol* **107**:110–115 (2012). https://doi.org/10.1016/j.biortech.2011.12.038.

7 Lei Y, Du M, Kuntke P, Saakes M, van der Weijden R and Buisman CJN, Energy efficient phosphorus recovery by microbial electrolysis cell induced calcium phosphate precipitation. *ACS Sustain Chem Eng* **7**:8860–8867 (2019). https://doi.org/10.1021/acssuschemeng.9b00867.

8 Janicek A, Fan Y and Liu H, Design of microbial fuel cells for practical application: a review and analysis of scale-up studies. *Biofuels* **5**:79–92 (2014). https://doi.org/10.4155/bfs.13.69.

9 Dekker A, ter Heijne A, Saakes M, Hamelers HVM and Buisman CJN, Analysis and improvement of a scaled-up and stacked microbial fuel cell. *Environ Sci Technol* **43**:9038–9042 (2009). https://doi.org/10.1021/es901939r.

10 Clauwaert P, Mulenga S, Aelterman P and Verstraete W, Litre-scale microbial fuel cells operated in a complete loop. *Appl Microbiol Biotechnol* **83**:241–247 (2009). https://doi.org/10.1007/s00253-009-1876-0.

11 Aelterman P, Rabaey K, Pham HT, Boon N and Verstraete W, Continuous electricity generation at high voltages and currents using stacked microbial fuel cells. *Environ Sci Technol* **40**:3388–3394 (2006). https://doi.org/10.1021/es0525511.

12 Greenman J and Ieropoulos IA, Allometric scaling of microbial fuel cells and stacks: the lifeform case for scale-up. *J Power Sources* **356**:365–370 (2017). https://doi.org/10.1016/j.jpowsour.2017.04.033.

13 Zamora P, Georgieva T, Ter Heijne A, Sleutels THJA, Jeremiasse AW, Saakes M *et al.*, Ammonia recovery from urine in a scaled-up Microbial Electrolysis Cell. *J Power Sources* **356** :491–499 (2017). https://doi.org/10.1016/j.jpowsour.2017.02.089

14 Gude VG, Wastewater treatment in microbial fuel cells – an overview. *J Clean Prod* **122**:287–307 (2016). https://doi.org/10.1016/j.jclepro.2016.02.022.

15 Sleutels THJA, Ter Heijne A, Buisman CJN and Hamelers HVM, Bioelectrochemical systems: an outlook for practical applications. *ChemSusChem* **5**:1012–1019 (2012). https://doi.org/10.1002/cssc.201100732.

16 Logan BE, Wallack MJ, Kim K-Y, He W, Feng Y and Saikaly PE, Assessment of microbial fuel cell configurations and power densities. *Environ Sci Technol Lett* **2**:206–214 (2015). https://doi.org/10.1021/acs.estlett.5b00180.

17 Rozendal RA, Hamelers HVM, Rabaey K, Keller J and Buisman CJN, Towards practical implementation of bioelectrochemical wastewater treatment. *Trends Biotechnol* **26**:450–459 (2008). https://doi.org/10.1016/j.tibtech.2008.04.008.

18 Sleutels THJA, Hamelers HVM, Rozendal RA and Buisman CJN, Ion transport resistance in Microbial Electrolysis Cells with anion and cation exchange membranes. *Int J Hydrogen Energy* **34**:3612–3620 (2009). https://doi.org/10.1016/j.ijhydene.2009.03.004.

19 Freguia S, Rabaey K, Yuan Z and Keller J, Electron and carbon balances in microbial fuel cells reveal temporary bacterial storage behavior during electricity generation. *Environ Sci Technol* **41**:2915–2921 (2007). https://doi.org/10.1021/es062611i.

20 Deeke A, Sleutels THJA, Donkers TFW, Hamelers HVM, Buisman CJN and Ter Heijne A, Fluidized capacitive bioanode as a novel reactor concept for the Microbial Fuel Cell. *Environ Sci Technol* **49**:1929–1935 (2015). https://doi.org/10.1021/es503063n.

21 Jiang D and Li B, Novel electrode materials to enhance the bacterial adhesion and increase the power generation in microbial fuel cells (MFCs). *Water Sci Technol* **59**:557–563 (2009). https://doi.org/10.2166/wst.2009.007.

22 Sleutels THJA, Darus L, Hamelers HVM and Buisman CJN, Effect of operational parameters on Coulombic efficiency in bioelectrochemical systems. *Bioresour Technol* **102**:11172–11176 (2011). https://doi.org/10.1016/j.biortech.2011.09.078.

23 Schneuwly A and Gallay R, Properties and applications of supercapacitors: from the state-of-the-art to future trends. *Proceedings PCIM 2000*, Nürnberg, pp. 1–10 (2000).

24 Deeke A, Sleutels THJA, Hamelers HVM and Buisman CJN, Capacitive bioanodes enable renewable energy storage in microbial fuel cells. *Environ Sci Technol* **46**:3554–3560 (2012). https://doi.org/10.1021/es204126r.

25 Deeke A, Sleutels THJA, Ter Heijne A, Hamelers HVM and Buisman CJN, Influence of the thickness of the capacitive layer on the performance of bioanodes in Microbial Fuel Cells. *J Power Sources* **243**:611–616 (2013). https://doi.org/10.1016/j.jpowsour.2013.05.195.

26 Houghton J, Santoro C, Soavi F, Serov A, Ieropoulos I, Arbizzani C *et al.*, Supercapacitive microbial fuel cell: characterization and analysis for improved charge storage/delivery performance. *Bioresour Technol* **218** :552–560 (2016). https://doi.org/10.1016/j.biortech.2016.06.105

27 Santoro C, Soavi F, Serov A, Arbizzani C and Atanassov P, Self-powered supercapacitive microbial fuel cell: the ultimate way of boosting and harvesting power. *Biosens Bioelectron* **78**:229–235 (2016). https://doi.org/10.1016/j.bios.2015.11.026.

28 Soavi F, Bettini LG, Piseri P, Milani P, Santoro C, Atanassov P *et al.*, Miniaturized supercapacitors: key materials and structures towards autonomous and sustainable devices and systems. *J Power Sources* **326** :717–725 (2016). https://doi.org/10.1016/j.jpowsour.2016.04.131

29 Borsje C, Liu D, Sleutels THJA, Buisman CJN and ter Heijne A, Performance of single carbon granules as perspective for larger scale capacitive bioanodes. *J Power Sources* **325**:690–696 (2016). https://doi.org/10.1016/j.jpowsour.2016.06.092.

30 Feng C, Lv Z, Yang X and Wei C, Anode modification with capacitive materials for a microbial fuel cell: an increase in transient power or stationary power. *Phys Chem Chem Phys* **16**:10464–10472 (2014). https://doi.org/10.1039/c4cp00923a.

31 Rodrigo Quejigo J, Tejedor-Sanz S, Esteve-Núñez A and Harnisch F, Bed electrodes in microbial electrochemistry: setup, operation and characterization. *ChemTexts* **5**:4 (2019). https://doi.org/10.1007/s40828-019-0078-3.

32 Liu J, Zhang F, He W, Yang W, Feng Y and Logan BE, A microbial fluidized electrode electrolysis cell (MFEEC) for enhanced hydrogen production. *J Power Sources* **271**:530–533 (2014). https://doi.org/10.1016/j.jpowsour.2014.08.042.

33 Liu X, Wu J and Guo Q, Analysis of organic compounds' degradation and electricity generation in anaerobic fluidized bed microbial fuel cell for coking wastewater treatment. *Environ Technol* **38**:3115–3121 (2017). https://doi.org/10.1080/09593330.2017.1290147.

34 Wang X, Yue X and Guo Q, Production of electricity during wastewater treatment using fluidized-bed microbial fuel cells. *Chem Eng Technol* **37**:703–708 (2014). https://doi.org/10.1002/ceat.201300241.

35 Liu J, Zhang F, He W, Zhang X, Feng Y and Logan BE, Intermittent contact of fluidized anode particles containing exoelectrogenic biofilms for continuous power generation in microbial fuel cells. *J Power Sources* **261**:278–284 (2014). https://doi.org/10.1021/es204126r.

36 Li J, Ge Z and He Z, A fluidized bed membrane bioelectrochemical reactor for energy-efficient wastewater treatment. *Bioresour Technol* **167**:310–315 (2014). https://doi.org/10.1016/j.biortech.2014.06.034.

37 Tejedor-Sanz S, Ortiz JM and Esteve-Núñez A, Merging microbial electrochemical systems with electrocoagulation pretreatment for achieving a complete treatment of brewery wastewater. *Chem Eng J* **330**:1068–1074 (2017). https://doi.org/10.1016/j.cej.2017.08.049.

38 Oka S, *Fluidized Bed*. Available: http://www.thermopedia.com/content/46/ [21 September 2018].

Journal of Chemical Technology & Biotechnology published by John Wiley & Sons Ltd on behalf of Society of Chemical Industry.

39 Hjelmner UR and Larsson HF, Method for the filtration of a suspension or emulsion. US Patent 4126546B1 (1977).

40 Molenaar SD, Sleutels T, Pereira J, Iorio M, Borsje C, Zamudio JA *et al.*, In situ biofilm quantification in bioelectrochemical systems by using optical coherence tomography. *ChemSusChem* **11** :2171–2178 (2018). https://doi.org/10.1002/cssc.201800589

41 Zehnder AJB, Huser BA, Brock TD and Wuhrmann K, Characterization of an acetate-decarboxylating, non-hydrogen-oxidizing methane bacterium. *Arch Microbiol* **124**:1–11 (1980). https://doi.org/10.1007/BF00407022.

42 Liang P, Zhang C, Jiang Y, Bian Y, Zhang H, Sun X, *et al.*, Performance enhancement of microbial fuel cell by applying transient-state regulation. *Appl Energy* **185** :582–588 (2017). https://doi.org/10.1016/j.apenergy.2016.10.130

43 Wang Y, Wen Q, Chen Y, Yin J and Duan T, Enhanced performance of a microbial fuel cell with a capacitive bioanode and removal of Cr (VI) using the intermittent operation. *Appl Biochem Biotechnol* **180**:1372–1385 (2016). https://doi.org/10.1007/s12010-016-2173-x.

44 Aelterman P, Freguia S, Keller J, Verstraete W and Rabaey K, The anode potential regulates bacterial activity in microbial fuel cells. *Appl Microbiol Biotechnol* **78**:409–418 (2008). https://doi.org/10.1007/s00253-007-1327-8.

45 Sleutels THJA, Molenaar SD, Ter Heijne A and Buisman CJN, Low substrate loading limits methanogenesis and leads to high Coulombic efficiency in bioelectrochemical systems. *Microorganisms* **4**:7 (2016). https://doi.org/10.3390/microorganisms4010007.

46 Porada S, Zhao R, van der Wal A, Presser V and Biesheuvel PM, Review on the science and technology of water desalination by capacitive deionization. *Prog Mater Sci* **58**:1388–1442 (2013). https://doi.org/10.1016/j.pmatsci.2013.03.005.

47 Han L, Karthikeyan KG, Anderson MA and Gregory KB, Exploring the impact of pore size distribution on the performance of carbon electrodes for capacitive deionization. *J Colloid Interface Sci* **430**:93–99 (2014). https://doi.org/10.1016/j.jcis.2014.05.015.

48 Porada S, Borchardt L, Oschatz M, Bryjak M, Atchison JS, Keesman KJ, *et al.*, Direct prediction of the desalination performance of porous carbon electrodes for capacitive deionization. *Energy Environ Sci* **6** :3700–3712 (2013). https://doi.org/10.1039/c3ee42209g

49 Gryglewicz G, Machnikowski J, Lorenc-Grabowska E, Lota G and Frackowiak E, Effect of pore size distribution of coal-based activated carbons on double layer capacitance. *Electrochim Acta* **50**:1197–1206 (2005). https://doi.org/10.1016/j.electacta.2004.07.045.

50 Picioreanu C, van Loosdrecht MCM and Heijnen JJ, A theoretical study on the effect of surface roughness on mass transport and transformation in biofilms. *Biotechnol Bioeng* **68**:355–369 (2000). https://doi.org/10.1002/(SICI)1097-0290(20000520)68:4<355::AID-BIT1>3.0.CO;2-A.

51 Champigneux P, Renault-Sentenac C, Bourrier D, Rossi C, Delia M-L and Bergel A, Effect of surface nano/micro-structuring on the early formation of microbial anodes with *Geobacter sulfurreducens*: experimental and theoretical approaches. *Bioelectrochemistry* **121**:191–200 (2018). https://doi.org/10.1016/j.bioelechem.2018.02.005.

52 Pierra, M, Golozar M, Zhang X, Prévoteau A, De Volder M, Reynaerts D *et al.*, Growth and current production of mixed culture anodic biofilms remain unaffected by sub-microscale surface roughness. *Bioelectrochemistry* **122** :213–220 (2018). https://doi.org/10.1016/j.bioelechem.2018.04.002

53 Chong P, Erable B and Bergel A, Microbial anodes: what actually occurs inside pores? *Int J Hydrogen Energy* **44**:4484–4495 (2019). https://doi.org/10.1016/j.ijhydene.2018.09.075.

54 Santoro C, Babanova S, Artyushkova K, Cornejo JA, Ista L, Bretschger O *et al.*, Influence of anode surface chemistry on microbial fuel cell operation. *Bioelectrochemistry* **106** :141–149 (2015). https://doi.org/10.1016/j.bioelechem.2015.05.002

55 Guo K, Prévoteau A, Patil SA and Rabaey K, Engineering electrodes for microbial electrocatalysis. *Curr Opin Biotechnol* **33**:149–156 (2015). https://doi.org/10.1016/j.copbio.2015.02.014.

